

SLAC-PUB-2916  
LBL-14402  
May 1982  
(T/E)

**D MESON PRODUCTION IN  $e^+e^-$  ANNIHILATION  
AT ECM BETWEEN 3.8 AND 6.7 GeV\***

M.W. Coles<sup>1</sup>, G.S. Abrams, C.A. Blocker<sup>3</sup>, A. Blondel,  
W.C. Carithers, W. Chinowsky, S. Cooper<sup>4</sup>, W.E. Dieterle,  
J.B. Dillon, M.W. Eaton, G. Gidal, G. Goldhaber, A.D. Johnson,  
J.A. Kadyk, A.J. Lankford, R.E. Millikan, M.E. Nelson, C.Y. Pang,  
J.F. Patrick, J. Strait, G.H. Trilling, E.N. Vella, and I. Videau<sup>6</sup>

*Lawrence Berkeley Laboratory and Department of Physics  
University of California, Berkeley, California 94720*

M.S. Alam<sup>2</sup>, A. Boyarski, M. Breidenbach, D.L. Burke,  
J. Dorenbosch<sup>5</sup>, J.M. Dorfan, G.J. Feldman, M.E.B. Franklin,  
G. Hanson, K.A. Hayes<sup>5</sup>, T. Himel<sup>5</sup>, D.G. Hitlin<sup>9</sup>,  
R. Hollebeek, W. Innes, J. Jaros, P. Jenni<sup>5</sup>, R.R. Larsen,  
V. Luth, M.L. Perl, B. Richter, A. Roussarie<sup>6</sup>, D.L. Scharre,  
R.H. Schindler<sup>5</sup>, R.F. Schwitters<sup>3</sup>, J.L. Siegrist, H. Taureg<sup>5</sup>,  
M. Tonutti<sup>7</sup>, R.A. Vidal, J.M. Weiss, and H. Zaccone<sup>6</sup>

*Stanford Linear Accelerator Center  
Stanford University Stanford, California 94305*

**Abstract**

The Mark II detector at SPEAR has been used to study D meson production in  $e^+e^-$  annihilation at center of mass energies between 3.8 and 6.7 GeV. The neutral and charged D mesons are identified from their  $K^{\mp}\pi^{\pm}$  and  $K^{\mp}\pi^{\pm}\pi^{\pm}$  decay modes. Measurements of  $R_D$  and of the inclusive differential cross section  $s d\sigma/dz$  are presented. The quasi two body cross sections  $\sigma_{D\bar{D}}$ ,  $\sigma_{D^+\bar{D}^-}$ , and  $\sigma_{D^-\bar{D}^+}$  are derived from an overall fit to the D recoil spectra. No evidence was found for the associated production of charmed mesons and charmed baryons.

(Submitted to Physical Review D)

---

\*Work supported by the Department of Energy, Contracts DE-AC03-76SF00515 and DE-AC03-76SF00098.

<sup>1</sup>Present address: Carnegie-Mellon University, Pittsburgh, PA 15213.

<sup>2</sup>Present address: Vanderbilt University, Nashville, TN 37235.

<sup>3</sup>Present address: Harvard University, Cambridge, MA 02138.

<sup>4</sup>Present address: DESY, Hamburg, Federal Republic of Germany.

<sup>5</sup>Present address: EP Division, CERN, Geneva, Switzerland.

<sup>6</sup>Present address: CEN-Saclay, France.

<sup>7</sup>Present address: Universitat Bonn, Federal Republic of Germany.

<sup>8</sup>Present address: LPNHE Ecole Polytechnique, Palaiseau, France.

<sup>9</sup>Present address: California Institute of Technology, Pasadena, CA 91125

## I. Introduction

One of the most useful indicators of new phenomena in  $e^+e^-$  annihilation has been the energy dependence of  $R$ , the ratio of the hadronic to muon pair cross sections. At energies above the prominent  $\psi$  and  $\psi'$  peaks,  $R$  exhibits a complex energy dependence associated with the production of charmed particles. The production of charmed mesons has been studied at the  $\psi''$  and at higher energies. These studies<sup>1,2</sup> have determined the mass of the charged and neutral  $D$  and  $D^*$ , their spins<sup>3,4</sup>,  $D$  and  $D^*$  branching fractions<sup>5</sup> to various final states, and production cross sections<sup>6</sup> at various center of mass energies. In this paper we present the results of a study of  $D$  and  $D^*$  production at center of mass energies between 3.8 and 6.7 GeV using the SLAC-LBL Mark II detector at the storage ring SPEAR.

Our measurements are presented in the following way. In section II we summarize the relevant features of the detector. In section III, we discuss the measurement of the energy dependence of inclusive neutral and charged  $D$  production cross sections. In section IV we present more detailed results on the inclusive momentum spectrum of  $D$ 's at a center of mass energy of 5.2 GeV where substantial statistics were accumulated. In section V we give an upper limit for the cross section for the associated production process  $e^+e^- \rightarrow \Lambda_c \bar{D}N$ . Section VI discusses the "resonance region" in  $R$  between roughly 3.8 and 4.4 GeV. The energy dependence of the production cross sections for the exclusive reactions  $e^+e^- \rightarrow D\bar{D}$ ,  $e^+e^- \rightarrow D^*\bar{D}$  or  $\bar{D}^*D$ , and  $e^+e^- \rightarrow D^*\bar{D}^*$  is discussed, and measurements of the branching fractions for the decays of charged and neutral  $D^*$ 's to pions or photons are presented. Finally, the energy dependence of these exclusive cross sections is compared to that dependence predicted theoretically by the  $q\bar{q}$  potential model of Eichten et al.<sup>21</sup>

## II. Experimental Apparatus

The Mark II detector (see Figure 1) has been described in detail elsewhere<sup>7,8</sup>. We concentrate on relevant features. Starting at the interaction region a particle first traverses a corrugated stainless steel vacuum pipe and a set of trigger scintillation counters, which together comprise about .05 radiation lengths of material. It then traverses a 16 layer drift chamber, a hodoscope of 48 time of flight counters, and an aluminum solenoidal coil which produces a 0.42 T axial magnetic field. Beyond the coil are eight lead-liquid argon electromagnetic shower counter modules and two or three layers of muon identifiers, each layer consisting of 23 to 30 cm of iron and a set of proportional tubes.

Charged tracks are reconstructed from signals in the 16 cylindrical drift chamber layers. The azimuthal coordinates of charged tracks are measured to an rms accuracy of approximately 220 microns at each layer. The polar coordinates are determined from the 10 "stereo" layers oriented at approximately  $\pm 3^\circ$  to the beam axis. When a track can be constrained to pass through the vertex, the charged particle rms momentum resolution is  $\delta p/p = [(0.015)^2 + (0.005p)^2]^{1/2}$  where  $p$  is the transverse momentum in GeV/c. Without this constraint the coefficient of the momentum-dependent term is doubled. Tracks are required to come within 1 cm radially and within  $\pm 10$  cm longitudinally of the measured beam crossing point. To insure more uniform detection efficiency and optimum momentum resolution, tracks passing this selection were required to have  $|\cos\theta| < 0.75$ , where  $\theta$  is the angle relative to the beam axis at the production vertex. Measured momenta are corrected for  $dE/dx$  losses in material traversed before entering the drift chamber.

The time of flight (TOF) scintillation counters which surround the drift chamber provide timing information over  $75\%$  of  $4\pi$  sr. Each TOF counter is a

2.54 cm thick Pilot F scintillator, 3.44 m long, and is viewed on each end by an Amperex XP 2230 photomultiplier tube. The system was calibrated using isochronous light pulses from a nitrogen flashtube, brought to the center of each counter through 10 m long light fibers. Signals from the tubes are fed to 12-bit TDCs and ADCs, the latter allowing a pulse height correction to be made. These slewing corrections are calculated offline from Bhabha-scattered electrons and allow us to obtain a system resolution of 315 ps for hadrons.

The lead-liquid argon shower counter modules which surround the solenoid are used to detect photons and identify high-energy electrons. The modules are approximately 14 radiation lengths in depth, provide almost full  $2\pi$  azimuthal coverage about the beam direction, and cover 64% of  $4\pi$  sr. The rms energy resolution for photons above 500 MeV in the calorimeter is approximately  $12\%/\sqrt{E}$  (GeV), but deteriorates somewhat at lower energies due to the effect of the coil. The angular resolution for photons is approximately 8 mrad.

The detector trigger employs a track-finding hardware processor which requires at least one track to traverse the entire drift chamber and an additional track to cross at least 3 of the 5 inner layers. All  $D$  decays that we investigate have at least two charged tracks which traverse the entire chamber.

The luminosity of the data sample is monitored by a pair of small angle scintillator and shower counters. These counters are positioned at 22 mrad from the beam axis, and identify Bhabha-scattered electrons. The counters are calibrated against larger angle Bhabha events measured in the fiducial volume of the drift chamber and lead-liquid argon calorimeter.

$D$  mesons used in this analysis were observed in the detector as peaks in the invariant mass spectra of the decay modes  $D^0 \rightarrow K^-\pi^+$  and  $\bar{D}^0 \rightarrow K^+\pi^-$ , and  $D^\pm \rightarrow K^\mp\pi^\pm\pi^\pm$ . These modes were chosen because of their relatively large branching fractions and because the invariant mass distributions had a better

ratio of signal to background than other decay channels.

To detect  $D$ 's which decay in this way, we relied on the ability of the time of flight counters to discriminate between charged pions and charged kaons. A  $\pi-K$  separation of greater than  $1\sigma$  time difference was possible for tracks with a momentum less than  $1.35 \text{ GeV}/c$ . Similarly,  $\pi-p$  and  $K-p$  separation was achieved for particle momenta less than  $2.0 \text{ GeV}/c$ . Each track was assigned three weights corresponding to its possible identity as a pion, kaon, or proton (anti-proton). Each weight was proportional to the Gaussian probability that if the particle had the assumed identity, its measured flight time would have deviated from the predicted flight time as much as observed. The normalization was such that the sum of all weights corresponding to a given track was unity. A particle was considered to be a proton if it had a proton weight greater than 0.9, it was called a kaon if it had a kaon weight greater than 0.5, and it was called a pion otherwise. Particles also were considered to be pions if there was no time of flight information available for them.

We eliminate positively identified leptons as follows. A second set of time of flight weights was formed to discriminate between electrons (or positrons) and pions if the momentum of the particle was less than  $300 \text{ MeV}/c$ . Tracks with an electron weight greater than 0.8 were taken to be electrons. At momenta above  $300 \text{ MeV}/c$ , electron-pion discrimination was based on the longitudinal distribution of energy deposited in the liquid argon shower counters.<sup>9</sup> Above  $800 \text{ MeV}/c$ , muons were distinguishable in the muon range counters.

### III. The Inclusive $D$ Production Cross Section

We have measured the ratio of the inclusive  $D$  meson production cross section to the theoretical muon pair production cross section

$$R_D = \frac{\sigma(D^+) + \sigma(D^-) + \sigma(D^0) + \sigma(\bar{D}^0)}{\sigma(\mu^+\mu^-)}$$

for center of mass energies between 3.9 GeV and 6.7 GeV.

In this analysis we determine a model independent efficiency for detection of  $D$  mesons. A previous measurement<sup>10</sup> has shown that  $D$  meson production in  $e^+e^-$  annihilation is consistent with being entirely two body or quasi-two body below a center of mass energy of 4.4 GeV and more complex above this energy. For this reason we have determined momentum dependent detection efficiencies and studied their sensitivity to the details of these various production mechanisms.

The detection efficiencies were determined by using a Monte Carlo program to generate  $D$ 's at various momenta. The Monte Carlo is designed to represent the properties of the detector as closely as possible. The  $D$ 's were generated both in an isotropic angular distribution and in the distributions  $\frac{dN}{d\Omega} \sim 1 \pm \cos^2\Theta$  where  $\Theta$  is the angle between the  $D$  momentum and  $e^+$  beam. The  $D$ 's were then allowed to decay, and the pions and kaons resulting from these decays were propagated through the detector. The pions and kaons were also allowed to decay, and tracks were reconstructed and selected to determine the detection efficiencies. The momentum dependence of the neutral and charged  $D$  detection efficiencies is shown in Figure 2. Even though Figure 2 indicates a difference of nearly 25% between the isotropic and anisotropic charged  $D$  detection efficiencies at 2 GeV/c, it was found from the substantial statistics accumulated at 5.2 GeV that the momentum distribution of  $D$ 's is peaked at low

momenta. That behavior minimizes this source of uncertainty.

In Figure 3 we show the  $K^{\mp}\pi^{\pm}$  and  $K^{\mp}\pi^{\pm}\pi^{\pm}$  invariant mass distributions in the  $D$  meson region for the accumulated data divided into two center of mass energy regions: 3.88-4.42 GeV (Figure 3a) and 4.5-6.0 GeV (Figure 3b). The widths ( $\sigma$ ) obtained from the fits to a Gaussian plus a polynomial background are  $17.2 \pm 1.7$  MeV ( $K\pi$ ),  $12.3 \pm 1.5$  MeV ( $K\pi\pi$ ) at the lower energies and  $13.8 \pm 2.1$  MeV ( $K\pi$ ),  $12.4 \pm 3.3$  MeV ( $K\pi\pi$ ) at the higher energies. The widths determined from the Monte Carlo program (17 MeV for  $K\pi$ , 15 MeV for  $K\pi\pi$ ) are consistent with these measurements and are almost independent of the  $D$  meson momentum.

We determined the amount of  $D$  production by analyzing our data in the following way. The numbers of charged and neutral  $D$ 's produced at a particular center of mass energy were determined from  $K^{\mp}\pi^{\pm}$  and  $K^{\mp}\pi^{\pm}\pi^{\pm}$  invariant mass distributions in various momentum bins. These invariant mass distributions for each momentum bin were fit to a Gaussian distribution plus a quadratic background. The center of the Gaussian was fixed at the known  $D$  mass, and its width was fixed to be the resolution width determined by the Monte Carlo simulation.

The number of produced  $D$ 's was determined by dividing the detected number of  $D$ 's (the results of the invariant mass fits) by the detection efficiency for isotropic production. The detection efficiency was evaluated at the center of the  $D$  momentum bin. The Mark II experiment has measured<sup>1</sup> the  $D^0 \rightarrow K^-\pi^+$  branching fraction and determined it to be  $0.03 \pm 0.06$ . The  $D^+ \rightarrow K^-\pi^+\pi^+$  branching ratio was determined to be  $0.063 \pm 0.011$ . These values were used to obtain the total numbers of produced  $D$ 's.

Systematic sources of uncertainty in the numbers of produced charged and neutral  $D$ 's are any deviation from the assumed isotropic production angular distribution and any variation of the detection efficiency over the range of each momentum slice. These sources of error together produced a systematic uncer-

tainty of less than 12% in the determination of the total number of neutral  $D$ 's produced and an uncertainty of, in general, less than 17% in the amount of charged  $D$  production. To calculate the inclusive  $D$  production cross section from the number of produced  $D$ 's, luminosities<sup>11</sup> based on wide angle Bhabha scattering were used. These luminosities have a systematic error of 6% which is negligible in relation to the other statistical and systematic sources of uncertainty.

The results are given in Table 1 and plotted in Figure 4. In the region below 4.5 GeV, we observe structure in the total  $R_D$ . Most of this structure comes from the excess of  $D^0$  over  $D^+$ , which is expected if most of the  $D$ 's come from  $D^*$  decay. The data were radiatively corrected according to the method of Bonneau and Martin.<sup>12</sup> These corrections are at most 15% near the 4 GeV structure and less than 5% elsewhere. In Figure 5 we compare the Mark II measurement of  $R$  (the usual ratio of total hadronic cross section to muon pair cross section),<sup>11,23</sup> with the sum of our measured value of  $R_D/2$  and 2.5. The number 2.5 ( $\pm 0.25$ ) is an estimate of the contribution from light ( $u,d,s$ ) quarks based on the various measured values of  $R$  below charm threshold.<sup>13</sup> From the comparison in Figure 5, we see that  $D$  production alone accounts for almost all of the charm contribution to  $R$  up to at least 6 GeV. The structure observed in  $R_D$  between 3.8 and 4.5 GeV is discussed in section VI.

One can use Figure 5 to set limits on the production cross section for the  $F$  meson and for charmed baryons at 5.2 GeV. We assume that the light quark ( $u,d,s$ ) contribution to  $R$  is 2.5, independent of cm energy, and that within statistical errors  $R$  is equal to  $R_D/2 + 2.5$ . The systematic errors (roughly 20% on  $R_D$ , 10% on the light quark contribution and 10% on  $R$  itself) then give a limit of one half unit of  $R$  for the pair production cross section of  $F$  mesons or charmed baryons. This is consistent with the Mark II measurement<sup>14</sup> of  $\Delta R \approx 0.3$  for charmed baryons above 5 GeV.

#### IV. Inclusive $D$ Production at 5.2 GeV

The availability of a large data sample at 5.2 GeV made it feasible to investigate in some detail the charm production characteristics at that center of mass energy. In particular, we measured the differential distribution in the scaling variable  $z$ , the ratio of total energy of the  $D$  meson to the beam energy. The kinematic limits imposed by the large  $D$  mass are that  $0.72 \leq z \leq 1$ .

We determined the quantity  $s d\sigma/dz$  in the same way as in section III, fitting  $K^\pm\pi^\mp$  and  $K^\mp\pi^\pm\pi^\pm$  invariant mass spectra within  $z$  bins of 0.05 units width to Gaussian distributions of fixed mean and width, plus quadratic backgrounds. As usual,  $s$  is the square of the center of mass energy. The detection efficiencies of Figure 2 and the branching fractions measured in the Mark II detector for  $D^0 \rightarrow K^-\pi^+$  and  $D^+ \rightarrow K^-\pi^+\pi^+$  were then used to determine  $s d\sigma/dz$ . The individual fits are shown in Figures 6 and 7 and the results are shown in Figure 8.

It is apparent that the quasi-two-body production processes  $D\bar{D}$ ,  $D^*\bar{D} + \bar{D}^*D$ , and  $D^*\bar{D}^*$  are not the dominant sources of  $D$ 's at 5.2 GeV, since for such processes  $D$ 's must have  $z > 0.93$ . The data of Figure 8 indicate that less than 35% (90% confidence level) of  $D^\pm$  production and less than 20% (90% confidence level) of  $D^0$  production occurs this way.<sup>15</sup>

Figure 9 compares the distribution in  $s d\sigma/dz$  observed for  $D^0$  production at 5.2 GeV with the same quantity observed in  $e^+e^-$  production of  $\pi^\pm$  and  $K_s^0$  between 6.1 and 7.6 GeV.<sup>17</sup> Apart from the lowest and highest  $z$  bins, the slope of the  $D^0$  spectrum has a value consistent with that observed for  $\pi^\pm$  and  $K_s^0$ .

We have parameterized the  $D^0$  spectrum in the form  $s d\sigma/dz = A(1-z)^n$ , and, ignoring the threshold bin, obtained  $n = 0.9 \pm 0.4$ . This value of  $n$  is in agreement with the previously reported<sup>18</sup> value of  $0.76^{+45}_{-33}$  obtained by the Mark I experiment at a center of mass energy of 7.0 GeV. Since 5.2 GeV is rather close to  $D\bar{D}$  threshold this distribution is severely constrained by kinematic

effects and is thus not expected to accurately reflect the  $D$  fragmentation function at asymptotic energies.

## V. Associated Production of Charmed Baryons and Charmed Mesons

We have previously reported<sup>14</sup> the observation of inclusive charmed baryon ( $\Lambda_c$ ) production in  $e^+e^-$  annihilation at 5.2 GeV. At 5.2 GeV, it is kinematically possible for the reactions  $e^+e^- \rightarrow \Lambda_c \bar{D}^0 \bar{p}$  and  $e^+e^- \rightarrow \Lambda_c D^- \bar{n}$  (or the charge conjugate states) to occur. The identification of a  $D$  meson and a proton or anti-proton in the same event would prove the existence of one of these reactions as the threshold for  $e^+e^- \rightarrow p\bar{p}D\bar{D}$  is about 5.6 GeV.

Two methods were used to search for these associated production processes. The first method required the detection of a  $D$  and the directly produced proton or anti-proton, while the second method required the detection of the  $D$  and a proton from the decay of the charmed baryon.

To employ the first method, the effective mass recoiling against the detected  $\bar{D}^0 \bar{p}$  system (or its charge conjugate) was calculated. Such a system was defined as a  $K^{\mp} \pi^{\pm}$  or  $K^{\mp} \pi^{\pm} \pi^{\pm} \pi^{\mp}$  mass combination in the range  $1.82 \text{ GeV}/c^2$  to  $1.90 \text{ GeV}/c^2$  plus a particle identified by time of flight as being a  $p$  or  $\bar{p}$ . Only 13 such events were observed in the data sample of  $5150 \text{ nb}^{-1}$ , and of these 13 events, none were observed to have a missing mass within  $200 \text{ MeV}/c^2$  of the  $\Lambda_c$  mass<sup>18</sup> ( $2.284 \text{ GeV}/c^2$ ). This gives a limit on associated production of less than  $0.4 \text{ nb}$  (0.12 units of  $R$ ) at the 90% confidence level.

In the second method for determining the existence of associated production, events were counted which contained a  $p$  and a  $\bar{D}$  or a  $\bar{p}$  and a  $D$ . The  $D$  was observed through the decays  $D^0 \rightarrow K^{\mp} \pi^{\pm}$ ,  $K^{\mp} \pi^{\pm} \pi^{\mp} \pi^{\pm}$ , and  $D^{\pm} \rightarrow K^{\mp} \pi^{\pm} \pi^{\pm}$ . Events were labeled as having a  $D$  if the invariant mass of the  $K$  and  $\pi$ 's was between

1.82  $\text{GeV}/c^2$  and 1.90  $\text{GeV}/c^2$ . A background subtraction was made using invariant mass combinations in the range of 1.65  $\text{GeV}/c^2$  to 1.69  $\text{GeV}/c^2$  or in the range between 2.03  $\text{GeV}/c^2$  and 2.07  $\text{GeV}/c^2$ . Events in both the signal and the sidebands were required to have a  $p$  or  $\bar{p}$  which was identified by time of flight with proton weight  $> 0.9$ . Sixteen such events were found containing a  $p$  or  $\bar{p}$  in the signal region and 17 such events were found in the sidebands, leaving no evidence for associated production after background subtraction. From the branching ratios<sup>1,18</sup> for  $D$  decay to  $K^-\pi^+$ ,  $K^+\pi^-\pi^+\pi^-$ , and  $K^-\pi^+\pi^+$ , and an isospin statistical model estimate that the fraction of  $\Lambda_c$  decays that lead to a proton is 0.6, an upper limit on associated production is estimated to be 0.4 nb, the same as for the first method.

## VI. Exclusive Channels in $D$ Meson Production

In the 4 GeV region, three  $D$  production modes have been observed:<sup>10</sup>

- (1)  $e^+e^- \rightarrow D\bar{D}$
- (2)  $e^+e^- \rightarrow D^*\bar{D}$  or  $\bar{D}^*D$
- (3)  $e^+e^- \rightarrow D^*\bar{D}^*$

With the same data sample as in section III, the relative rates of production of these three channels were measured at center of mass energies between 3.9 GeV and 4.3 GeV. For the analysis of the exclusive channels, an event was said to be a  $D$  candidate if the  $K^-\pi^\pm$  or  $K^+\pi^\pm\pi^\pm$  invariant mass was between 1.82  $\text{GeV}/c^2$  and 1.90  $\text{GeV}/c^2$ .

Because of the limited data sample available and the small branching fractions for  $D^0 \rightarrow K^-\pi^+$  and  $D^+ \rightarrow K^-\pi^+\pi^+$ , at most one  $D$  meson was detected in each event containing charm. To establish which of the three reactions was the mechanism for production of a particular  $D$ , the recoil effective mass opposite

the  $D$  was calculated. If the  $D$  is directly produced, rather than the result of a  $D^*$  decay, the observed recoil mass spectrum should be populated only around the  $D$  and  $D^*$  masses smeared by the detector's momentum resolution. If the detected  $D$  is the result of  $D^*$  decay, the distribution in effective recoil mass observed is more complicated. The shape of the distribution then depends on the angular distribution of the decay  $D$  about the direction of motion of the parent  $D^*$ . Using angular momentum conservation, one can show that in reaction (2) the production angular distribution of the  $D$  meson with respect to the  $D^*$  helicity axis is of the form  $\frac{dN}{d\Omega} \sim 1 + \alpha \cos^2 \Theta$ , with  $\alpha = +1$  for  $D^* \rightarrow \gamma D$  and  $\alpha = -1$  for  $D^* \rightarrow \pi D$ . For reaction (3), the angular distribution is again of the form  $\frac{dN}{d\Omega} \sim 1 + \alpha \cos^2 \Theta$  if  $F$  wave production is ignored. The parameter  $\alpha$  is not calculable in (3) as it depends on the ratio of the  $^1P$  and  $^5P$  production amplitudes, and also on the decay mode of the undetected  $D^*$ .

The rates for reactions (1)-(3) were determined by fitting<sup>22</sup> the recoil effective mass squared spectrum in two ways. The first method assumed that the angular distribution of a  $D$  relative to the direction of motion of its parent  $D^*$  was isotropic in reaction (3). The second method allowed for an angular dependence of the form

$$\frac{dN}{d\Omega} \sim 1 + \alpha \cos^2 \Theta$$

as mentioned earlier, where  $\alpha$  was determined by the fitting program for reaction (3). The angular dependence was assumed to be energy independent, but different  $\alpha$ 's were allowed for the different decay modes of the  $D^*$ . It was also assumed that the intermediate photon produced in the  $e^+e^-$  annihilation coupled directly to the  $c\bar{c}$  quark pair which produced the observed  $D$  meson. Since that implies the  $D$ 's are in a pure isospin zero state, the cross sections are related by:

$$\sigma_{D^0\bar{D}^0} = \sigma_{D^+D^-} \left( \frac{p_{D^0}}{p_{D^+}} \right)^3.$$

$$\sigma_{D^{*0}\bar{D}^0} = \sigma_{D^{*+}D^-} \left( \frac{p_{D^{*0}}}{p_{D^{*+}}} \right)^3.$$

$$\sigma_{D^{*0}\bar{D}^{*0}} = \sigma_{D^{*+}D^{*-}} \left( \frac{p_{D^{*0}}}{p_{D^{*+}}} \right)^3.$$

The  $p^3$  factors account for phase space differences in the production of charged and neutral  $D$ 's produced in  $l=1$  states. Finally, it was assumed that

$$B(D^{*+} \rightarrow D^0\pi^+) + B(D^{*+} \rightarrow D^+\pi^0) + B(D^{*+} \rightarrow D^+\gamma) = 1,$$

$$B(D^{*0} \rightarrow D^0\pi^0) + B(D^{*0} \rightarrow D^0\gamma) = 1 ..$$

The expected distribution of  $D$ 's was convoluted with detector resolution to obtain the fitting functions for neutral and charged  $D$ 's as:

$$\begin{aligned}
dN^0 &= L \Delta M_R^2 \varepsilon_{K\pi} (M_R^2) B(D^0 \rightarrow K^-\pi^+) \left[ 2\sigma_{D^0 D^0} + \right. \\
&\quad \sigma_{D^* D^0} \left[ C_2^0 + B(D^{*0} \rightarrow D^0\pi^0) C_1^0 + B(D^{*0} \rightarrow D^0\gamma) C_4^0 + B(D^{*+} \rightarrow D^0\pi^+) C_3^0 \left( \frac{p_{D^+}}{p_{D^0}^3} \right) + \right. \\
&\quad \left. \left. 2\sigma_{D^* D^*} \left[ B(D^{*0} \rightarrow D^0\pi^0) C_5^0 + B(D^{*0} \rightarrow D^0\gamma) C_7^0 + B(D^{*+} \rightarrow D^+\pi^0) C_8^0 \left( \frac{p_{D^{*+}}}{p_{D^*}^3} \right)^3 \right] \right] + Q^0
\right. \\
dN^+ &= L \Delta M_R^2 \varepsilon_{K\pi\pi} \left[ 2\sigma_{D^0 D^0} \left( \frac{p_{D^+}}{p_{D^0}} \right)^3 C_0^+ + \right. \\
&\quad \sigma_{D^* D^0} \left( \frac{p_{D^+}}{p_{D^0}} \right)^3 [B(D^{*+} \rightarrow D^+\gamma) C_3^+ + B(D^{*+} \rightarrow D^+\pi^0) C_1^+ + C_2^+] + \\
&\quad \left. 2\sigma_{D^* D^*} \left( \frac{p_{D^{*+}}}{p_{D^*}} \right)^3 [B(D^{*+} \rightarrow D^+\gamma) C_4^+ + B(D^{*+} \rightarrow D^+\pi^0) C_5^+] \right] + Q^+
\end{aligned}$$

where  $Q^0$  and  $Q^+$  are quadratic parameterizations of the backgrounds and the other parameters are defined in the Appendix. To check this fitting function, a Monte Carlo model was constructed which generated reactions (1), (2), and (3) and the subsequent  $D^*$  decays according to the matrix elements given by Cahn and Kayser.<sup>19</sup> The distribution of neutral  $D$ 's produced by the Monte Carlo at a center of mass energy of 4.16 GeV is shown in Figure 10 together with the function fitted to the recoil mass squared distribution. The fitting procedure accurately reproduced the input parameters of the Monte Carlo.

To increase the statistical accuracy of the fitting procedure, a simultaneous  $\chi^2$  minimization was done to eight different data sets. These consisted of the recoil mass squared spectra opposite both charged and neutral  $D$ 's in the four center of mass energy regions  $3.88 \text{ GeV} \leq E_{cm} \leq 4.02 \text{ GeV}$ ,  $4.02 \text{ GeV} \leq E_{cm} \leq 4.15 \text{ GeV}$ ,  $E_{cm} = 4.16 \text{ GeV}$ , and  $4.15 \text{ GeV} \leq E_{cm} \leq 4.3 \text{ GeV}$  exclusive of the 4.16 GeV

data.

The results of this fitting are given in Tables 2 and 3 and shown for the isotropic fit to the data from 4.02 to 4.15 GeV in Figure 11. The fact that the results of the anisotropic and isotropic fits are nearly identical indicates that the results obtained are relatively insensitive to the exact form of the production matrix element. As a consistency check, the inclusive value of  $R_D$  from section III is compared with the value of  $R_D$  obtainable from Table 2. The comparison of these cross sections is shown in Table 4. The value of  $R_D$  resulting from the exclusive channel analysis requires that  $R_D$  be the result of reactions (1), (2), and (3), only. The good agreement between the two methods indicates that the background parameterization used in the exclusive channel fits is reasonable, especially since the two methods for determining the background were completely independent. In the inclusive analysis, the background was determined from the shape of the  $D$  invariant mass spectrum in  $D^0$  or  $\bar{D}^0 \rightarrow K \pi$  and  $D^\pm \rightarrow K \pi^\pm \pi^\pm$  while for the exclusive decays, the background determination came entirely from the parameterization of the recoil mass spectrum opposite the  $D$ . The branching ratios for  $D^*$  decay determined by the fit are shown in Table 3 and are in good agreement with the previously reported Mark I results.<sup>1</sup>

Soon after the discovery of the  $D$  it was suggested that the relative ratios of reactions (1), (2), and (3) could be described by simply counting the number of spin states available to each reaction.<sup>20</sup> This reasoning predicts the relative ratios of these reactions as

$$\sigma_{D\bar{D}} : \sigma_{D^* \bar{D}} : \sigma_{D^* \bar{D}^*} = p_{D,\bar{D}}^3 : 4p_{D^*,\bar{D}}^3 : 7p_{D^*,\bar{D}^*}^3$$

At a center of mass energy of 4.16 GeV, this argument predicts the ratio 1:2.2:1.45 in contrast to the experimentally observed ratio of  $(1.0 \pm 0.6):(4.6 \pm 1.2):(9.8 \pm 1.6)$ . A way to explain this ratio by introducing dynamical arguments has been presented by Eichten et al.<sup>21</sup> They postulate production

of quark-antiquark pairs, attracted by a potential of the form  $V(r) = -k/r + r/a^2$  where  $r$  is the  $q\bar{q}$  separation. Rates were calculated according to non-relativistic quantum mechanical rules assuming that the virtual photon produced in  $e^+e^-$  annihilation couples directly to the  $c-\bar{c}$  pair. The model parameters are determined from the observed charmonium states. Figure 12 shows the predictions of this model for the energy dependence of the cross sections which describe reactions (1), (2), and (3). Overplotted are the results of the isotropic fit given in Table 2 for these reactions. The relative magnitudes observed are in approximate agreement with this model.  $D\bar{D}$  production is suppressed at all energies while  $D^*\bar{D}^*$  production accounts for the bulk of observed  $D$ 's over the entire center of mass energy region from 3.9 GeV to 4.3 GeV. Agreement between the model and the observed  $D\bar{D}$  and  $D^*\bar{D} + \bar{D}^*D$  production cross sections is good in all four energy bins.

## VII. Summary and Conclusion

The  $D$  meson production cross section has been measured at center of mass energies between 3.88 and 6.7 GeV. The comparison of this cross section to the total hadronic cross section leads one to conclude that  $D$  production accounts for almost all the charm contribution to the total hadronic cross section in this energy region. Over the limited kinematic range available, the inclusive differential cross section  $s d\sigma/dz$  at 5.2 GeV is well described by the simple parameterization  $s d\sigma/dz = A(1-z)^n$  with  $n = 0.9 \pm 0.4$ . No evidence was found for the associated production of charmed mesons and charmed baryons at 5.2 GeV. An upper limit for this cross section is 0.4 nb at the 90% confidence level. The energy dependences of the quasi-two-body production cross sections  $\sigma_{D\bar{D}}$ ,  $\sigma_{D^*\bar{D}^*}$ , and  $\sigma_{D^*\bar{D}}$  were measured between 3.88 GeV and 4.3 GeV. The exclusive two body cross sections were found to have an energy dependence

which is in reasonable agreement with the dependence predicted by Eichten et al.<sup>14</sup> as a dynamical consequence of a quark-antiquark binding potential. The branching fractions for  $D^*$  decay to  $D\pi$  and  $D\gamma$  were found to be in agreement with previous results.<sup>10</sup>

### **Acknowledgments**

This work was supported in part by the Director, Office of Energy Research, Division of High Energy and Nuclear Physics of the U.S. Department of Energy under Contracts DE-AC03-76SF00098 and DE-AC03-76SF00515.

## APPENDIX

**Definition of Variables Appearing in the Fitting Functions**

| Variable                           | Definition   |
|------------------------------------|--|
| $L$                                | Integrated luminosity of data sample.  |
| $\varepsilon_{K\pi}(M_K^2)$        | Momentum dependent detection efficiency for $D^0 \rightarrow K^-\pi^+$ from Figure 2.      |
| $\varepsilon_{K\pi\pi}(M_K^2)$     | Momentum dependent detection efficiency for $D^- \rightarrow K^+\pi^-\pi^-$ from Figure 2. |
| $B(D^0 \rightarrow K^-\pi^+)$      | Branching fraction for $D^0 \rightarrow K^-\pi^+ = 0.03 \pm .006$ .                        |
| $B(D^+ \rightarrow K^+\pi^+\pi^+)$ | Branching fraction for $D^+ \rightarrow K^+\pi^+\pi^+ = 0.063 \pm .011$ .                  |
| $B(D^* \rightarrow X)$             | Branching fraction for $D^*$ decay to state X.   |
| $\Delta M_K^2$                     | Bin width of data in $dN/dM_K^2$ distribution.   |

Recoil Mass Distributions  $dN/dM_R^2$ 

| Distribution | Event Type   |
|--------------|--|
| $C_0^0$      | $e^+e^- \rightarrow D^{*0}\bar{D}^0$                           |
| $C_1^0$      | $\rightarrow D^{*0}\bar{D}^0, D^{*0} \rightarrow D^0\pi^0$     |
| $C_2^0$      | $\rightarrow D^0\bar{D}^{*0}$                                  |
| $C_3^0$      | $\rightarrow D^{*+}D^-, D^{*+} \rightarrow D^0\pi^+$           |
| $C_4^0$      | $\rightarrow D^{*0}\bar{D}^0, D^{*0} \rightarrow D^0\gamma$    |
| $C_5^0$      | $\rightarrow D^{*0}D^{*0}, D^{*0} \rightarrow D^0\pi^0$        |
| $C_6^0$      | $\rightarrow D^{*+}D^{*-}, D^{*+} \rightarrow D^0\pi^+$        |
| $C_7^0$      | $\rightarrow D^{*0}\bar{D}^{*0}, D^{*0} \rightarrow D^0\gamma$ |
| $C_0^+$      | $\rightarrow D^+D^-$   |
| $C_1^+$      | $\rightarrow D^{*+}D^-, D^{*+} \rightarrow D^+\pi^0$           |
| $C_2^+$      | $\rightarrow D^+D^{*-}$  |
| $C_3^+$      | $\rightarrow D^{*+}D^-, D^+\gamma$                             |
| $C_4^+$      | $\rightarrow D^{*+}D^{*-}, D^{*+} \rightarrow D^+\gamma$       |
| $C_5^+$      | $\rightarrow D^{*+}D^{*-}, D^{*+} \rightarrow D^+\pi^0$        |

Each distribution is normalized to unity when integrated over the possible kinematic range. Each process refers to the charge conjugate process as well. For ease in defining the distributions, a  $D^0$  is the detected particle in all the  $C^0$  distributions and a  $D^+$  is the detected particle in the  $C^+$  distributions.

## REFERENCES

1. R.H. Schindler et al., *Phys. Rev. D24*, 78 (1981).
2. P.A. Rapidis et al., *Phys. Rev. Lett.* **39**, 526 (1977); H.F.W. Sadrozinski, invited talk at the XXth International Conference on High Energy Physics, University of Wisconsin, Madison, WI, (1980). SLAC-PUB-2589.
3. H.K. Nguyen et al., *Phys. Rev. Lett.* **39**, 262 (1977).
4. I. Peruzzi et al., *Phys. Rev. Lett.* **39**, 1301 (1977).
5. Ref. 1 gives branching fractions for  $D$  decays. See also G. Abrams et al.; *Phys. Rev. Lett.* **43**, 481 (1979) and ref. 4. Measurements of  $D^*$  branching fractions are given in ref. 9.
6. M. Piccolo et al., *Phys. Lett.* **86B**, 220 (1979).
7. W. Davies-White et al., *Nucl. Instrum. Meth.* **160**, 227 (1979).
8. G.S. Abrams et al., *Phys. Rev. Lett.* **43**, 477 (1979), G.S. Abrams et al., *Phys. Rev. Lett.* **43**, 481 (1979).
9. G.S. Abrams et al., *IEEE Trans. Nucl. Sci.* **27**, 59 (1980).
10. G. Goldhaber et al., *Phys. Lett.* **69B**, 503 (1977).
11. J.L. Siegrist, SLAC-225, 1979, Ph.D. thesis.
12. G. Bonneau and F. Martin, *Nucl. Phys.* **B27**, 381 (1971).
13. J. Burmester et al., *Phys. Lett.* **66B**, 395 (1977); R. Brandelik et al., *Phys. Lett.* **76B**, 361 (1978); and J. Kirkby et al., *Proceedings of the SLAC Summer Institute on Particle Physics*, 1978, edited by M. Zipf, SLAC-215; J.L. Siegrist et al., SLAC-PUB-2831, LBL-13464 (October 1981), submitted to *Physical Review D*.
14. G.S. Abrams et al., *Phys. Rev. Lett.* **44**, 10 (1980).
15. We have attempted to determine the number of particles produced in association with the two  $D$  mesons at 5.2 GeV by comparing the produced charged particle multiplicity distribution observed opposite a  $D$  candidate at this energy with the distribution observed at 3.77 GeV. The distribution at 5.2 GeV contains a very large uncertainty due to background subtractions causing the comparison of the distributions to be of little statistical significance.
16. P.A. Rapidis et al., *Phys. Lett.* **84B**, 507 (1979). See also ref. 6.

17. V. Luth et al., Phys. Rev. Lett. *70B*, 120 (1977); V. Luth in Proceedings of the SLAC Summer Institute on Particle Physics, 1977, edited by M. Zipf, SLAC-204; G. Hanson in Proceedings of the 13th Recontre de Moriond on High Energy Leptonic Interactions and High Energy Hadronic Interactions, Les Arcs, Savoie, France, 1977, edited by Tran Tranh Van.
18. The Mark II determined branching ratio for  $D^0 \rightarrow K^-\pi^+\pi^-\pi^+$  from reference 1 was used in this calculation;  $B(D^0 \rightarrow K^-\pi^+\pi^-\pi^+) = 8.5 \pm 2.1 \%$ .
19. R. Cahn and B. Kayser, Phys. Rev. *D22*, 2752 (1980).
20. F.E. Close, Phys. Lett. *65*, 55 (1976).
21. E. Eichten et al., Phys. Rev. *D21*, 203 (1980).
22. Further details of the fitting procedure are given in M. Coles, LBL-11513, 1980. Ph.D. thesis.
23. R.H. Schindler et al., Phys. Rev. *D21*, 2716 (1980).

**TABLES**

1. Measured  $R_D$  for each energy interval.
2. Two body cross sections from recoil mass fits.
3. Branching ratios from recoil mass fits.
4. Comparison of Inclusive  $D$  cross section obtained from invariant mass fits and those obtained from recoil mass fits.

## FIGURE CAPTIONS

1. Cross sectional view of the Mark II detector.
2. Momentum dependent detection efficiencies for: (a)  $D^0 \rightarrow K^-\pi^+$ , (b)  $D^+ \rightarrow K^-\pi^+\pi^+$ . Both diagrams show the effects of angular distribution in the production angle of a  $D$  with respect to the beam direction. The solid lines are our parameterizations of the isotropic production detection efficiencies.
3. The  $K^+\pi^\pm$  and  $K^+\pi^\pm\pi^\pm$  invariant mass distributions for accumulated data at center of mass energies (a) between 3.88 and 4.42 GeV, and (b) between 4.5 and 6.0 GeV. The curves are the results of a fit to a Gaussian plus a polynomial background.
4. The energy dependence of the inclusive  $D$  production cross section divided by the muon pair production cross section for: (a) neutral  $D$ 's alone, (b) charged  $D$ 's alone, and (c) charged and neutral  $D$ 's together. A data point from ref. 16 (MKI) is also shown.
5. Comparison of one half the inclusive  $D$  production cross section divided by the muon pair production cross section plus 2.5 to the total pair production ( $R$ ). 2.5 is approximately the value of  $R$  below charm threshold.
6. Invariant mass spectra for  $K^+\pi^-$  combinations for 6 regions of  $z = 2E_D/\sqrt{s}$ . The lines are our fits to the expected  $D^0 \rightarrow K^-\pi^+$  mass spectra and are described in the text.
7. Invariant mass spectra for  $K^+\pi^\pm\pi^\pm$  combinations for 6 regions of  $z = 2E_D/\sqrt{s}$ . The lines are our fits to the expected  $D^+ \rightarrow K^-\pi^+\pi^+$  mass spectra and are described in the text.
8. The differential scaling cross section  $s d\sigma/dz$  measured at a center of mass energy of 5.2 GeV for (a) neutral  $D$ 's and (b) charged  $D$ 's.
9. Comparison of the differential scaling cross section  $s d\sigma/dz$  for neutral  $D$ 's produced at a center of mass energy of 5.2 GeV (Mark II) to that observed for charged pions and neutral kaons produced between 6.1 and 7.8 GeV (Mark I).
10. The Monte Carlo produced recoil mass squared spectrum produced opposite a detected neutral  $D$  at a center of mass energy of 4.16 GeV. The uppermost curve is a fit to the spectrum using the fitting function described in the text. The numbered curves show contributions from the processes: (1)  $D^0\bar{D}^0$ , (2)  $D^0\bar{D}^0\gamma$ , (3)  $D^+\bar{D}^-$ ,  $D^+\rightarrow D^0\pi^+$ , (4)  $D^0\bar{D}^0$ ,  $D^0\rightarrow D^0\pi^0$ , (5)  $D^0\bar{D}^0$ ,  $D^0\rightarrow D^0\gamma$ , (6)  $D^0\bar{D}^0$ ,  $D^0\rightarrow D^0\gamma$ , (7)  $D^0\bar{D}^0$ ,  $D^0\rightarrow D^0\pi^0$ , (8)  $D^+\bar{D}^-$ ,  $D^+\rightarrow D^0\pi^+$ . The double peak near  $4.6 \text{ GeV}^2/c^4$  is a consequence of the angular distribution of the  $D^0$  with respect to the  $D^+$  helicity axis.

11. Two of the eight recoil spectra simultaneously fit using the recoil distribution function described in the text. The data shown were taken at center of mass energies between 4.02 and 4.15 GeV.
12. Comparison of the energy dependence of the exclusive  $D$  production cross sections observed to that predicted by the model of Eichten et al.<sup>21</sup>

| Energy<br>(GeV) | Luminosity<br>(nb <sup>-1</sup> ) | No. of Events<br>$D^-$ | No. of Events<br>$D^0$ | $\sigma_{\pm} \cdot B(D^- \rightarrow K^- \pi^+ \pi^+)$<br>(nb) | $\sigma_0 \cdot B(D^0 \rightarrow K^- \pi^+ \pi^+)$<br>(nb) | $\sigma_{\pm}$<br>(nb) | $\sigma_0$<br>(nb) | $R_D$            |
|-----------------|-----------------------------------|------------------------|------------------------|---|---|------------------------|--------------------|------------------|
| 3.88 - 4.02     | 374                               | 18 ± 9                 | 23 ± 6                 | .25 ± .13   | .17 ± .04   | 4.0 ± 2.1              | 5.7 ± 1.3          | 1.7 ± .4         |
| 4.02 - 4.15     | 906                               | 41 ± 12                | 152 ± 15               | .29 ± .08   | .54 ± .06   | 4.6 ± 1.3              | 18.0 ± 2.0         | 4.3 ± .5         |
| 4.16            | 1248                              | 42 ± 12                | 128 ± 14               | .19 ± .06   | .30 ± .03   | 3.0 ± 1.0              | 10.0 ± 1.0         | 2.6 ± .3         |
| 4.15 - 4.20     | 342                               | 17 ± 7                 | 45 ± 8                 | .27 ± .12   | .38 ± .07   | 4.3 ± 1.9              | 12.7 ± 2.3         | 3.4 ± .6         |
| 4.20 - 4.30     | 672                               | 25 ± 9                 | 40 ± 10                | .23 ± .06   | .17 ± .04   | 3.7 ± 1.0              | 5.7 ± 1.3          | 2.0 ± .4         |
| 4.30 - 4.40     | 221                               | 26 ± 8                 | 19 ± 9                 | .80 ± .25   | .34 ± .15   | 12.7 ± 4.0             | 11.3 ± 5.0         | 5.3 ± 1.4        |
| 4.40 - 4.42     | 1315                              | 54 ± 16                | 160 ± 18               | .25 ± .07   | .40 ± .05   | 4.0 ± 1.1              | 13.3 ± 1.7         | 3.9 ± .4         |
| 4.50 - 4.85     | 1565                              | 65 ± 17                | 65 ± 15                | .23 ± .06   | .13 ± .03   | 3.7 ± 1.0              | 4.3 ± 1.0          | 2.0 ± .4         |
| 4.85 - 5.20     | 1655                              | 57 ± 18                | 74 ± 17                | .27 ± .09   | .22 ± .05   | 4.3 ± 1.4              | 7.3 ± 1.7          | 3.3 ± .6         |
| 5.20            | 5110                              | 118 ± 33               | 241 ± 31               | .15 ± .04   | .18 ± .03   | 2.4 ± .6               | 6.0 ± 1.0          | 2.6 ± .4         |
| 5.20 - 6.00     | 753                               | 8 ± 12<br>- 4          | 30 ± 10                | .08 ± .09<br>- .04  | .19 ± .05   | 1.3 ± 1.4<br>- .6      | 6.3 ± 1.7          | 2.8 ± .8<br>- .6 |
| 6.5 - 6.70      | 3650                              | 44 ± 16                | 54 ± 17                | .10 ± .03   | .07 ± .02   | 1.6 ± .5               | 2.3 ± 0.7          | 2.0 ± .5         |

Table 1

Table 2. Fit Results

| Cross Section<br>(nb)    | Energy Region       |                     |               |                | Isotropic Fit   |
|--------------------------|---------------------|---------------------|---------------|----------------|-----------------|
|                          | 3.88 - 4.02 GeV     | 4.02 - 4.15 GeV     | 4.16 GeV      | 4.15 - 4.3 GeV |                 |
| $\sigma_{D\bar{D}}$      | $0.2^{+0.3}_{-0.2}$ | $0.3 \pm 0.3$       | $0.4 \pm 0.2$ | $0.3 \pm 0.3$  |                 |
| $\sigma_{D^* \bar{D}}$   | $2.7 \pm 0.7$       | $3.8 \pm 0.6$       | $2.0 \pm 0.4$ | $1.6 \pm 0.5$  |                 |
| $\sigma_{D^* \bar{D}^*}$ | --                  | $5.7 \pm 0.8$       | $4.4 \pm 0.6$ | $3.1 \pm 0.6$  |                 |
|                          |                     |                     |               |                |                 |
| $\sigma_{D\bar{D}}$      | $0.2^{+0.3}_{-0.2}$ | $0.2^{+0.3}_{-0.2}$ | $0.4 \pm 0.3$ | $0.3 \pm 0.3$  | Anisotropic Fit |
| $\sigma_{D^* \bar{D}}$   | $2.6 \pm 0.7$       | $3.7 \pm 0.7$       | $2.0 \pm 0.5$ | $1.6 \pm 0.5$  |                 |
| $\sigma_{D^* \bar{D}^*}$ | --                  | $5.9 \pm 1.2$       | $4.4 \pm 0.7$ | $3.2 \pm 0.8$  |                 |

Table 3

## Branching Ratios

| Mode                            | Isotropic Fit | Anisotropic Fit | Mark I Result |
|---------------------------------|---------------|-----------------|---------------|
| $D^{*0} \rightarrow D^0 \pi^0$  | .47 ± .09     | .53 ± .12       | .55 ± .15     |
| $D^{*0} \rightarrow D^0 \gamma$ | .53 ± .09     | .47 ± .12       | .45 ± .15     |
| $D^{*+} \rightarrow D^0 \pi^+$  | .44 ± .07     | .44 ± .10       | .60 ± .15     |
| $D^{*+} \rightarrow D^+ \pi^0$  | .28 ± .07     | .34 ± .07       | --            |
| $D^{*+} \rightarrow D^+ \gamma$ | .28 ± .10     | .22 ± .12       | --            |

**Inclusive D Production Cross Section  
Before Radiative Corrections**

| Energy<br>Region<br>(GeV) | Recoil<br>Method<br>(nb) | Inclusive<br>Method<br>(nb) |
|---------------------------|--------------------------|-----------------------------|
| 3.88 - 4.02               | $2.9 \pm .8$             | $4.9 \pm 1.3$               |
| 4.02 - 4.15               | $9.8 \pm 1.0$            | $9.4 \pm 1.0$               |
| 4.16                      | $6.8 \pm .7$             | $6.5 \pm .7$                |
| 4.15 - 4.30               | $5.1 \pm 1.0$            | $5.7 \pm 1.4$               |

Table 4

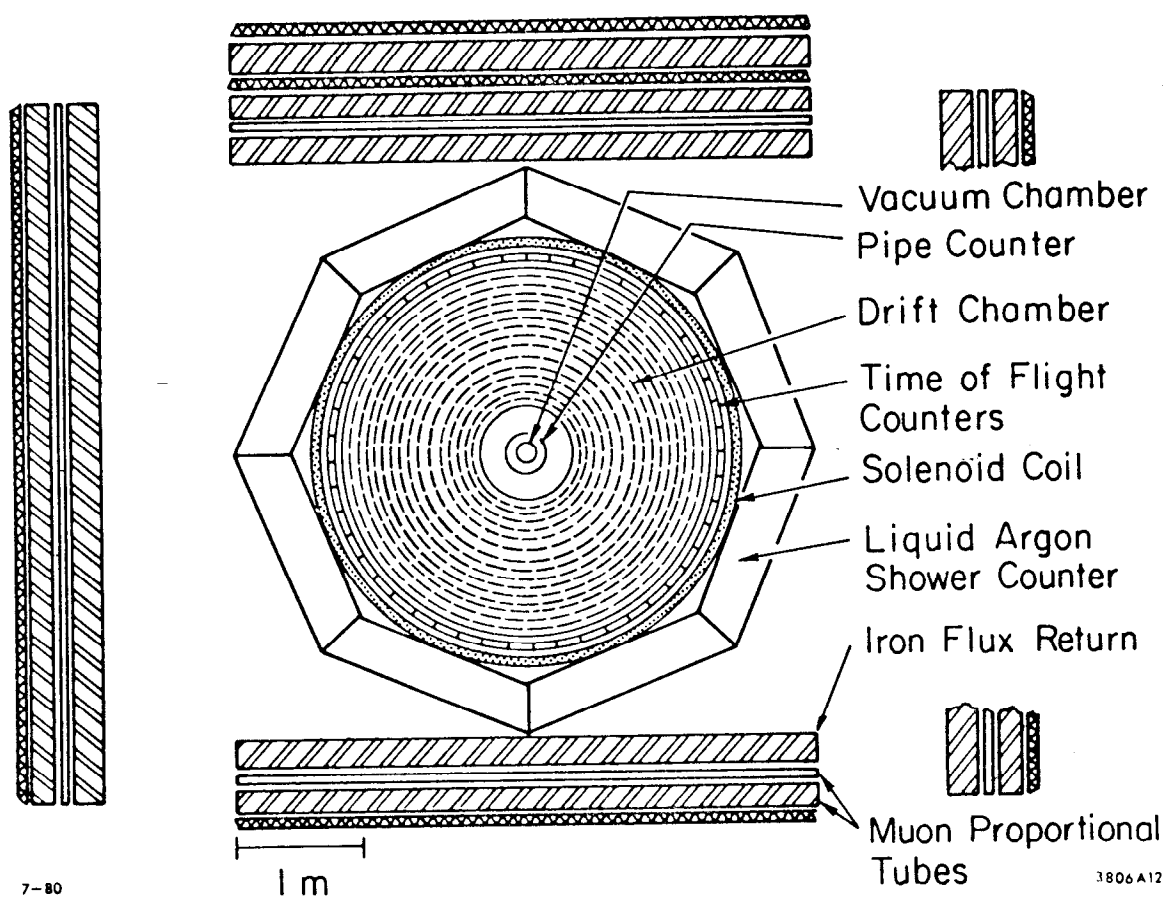


Fig. 1

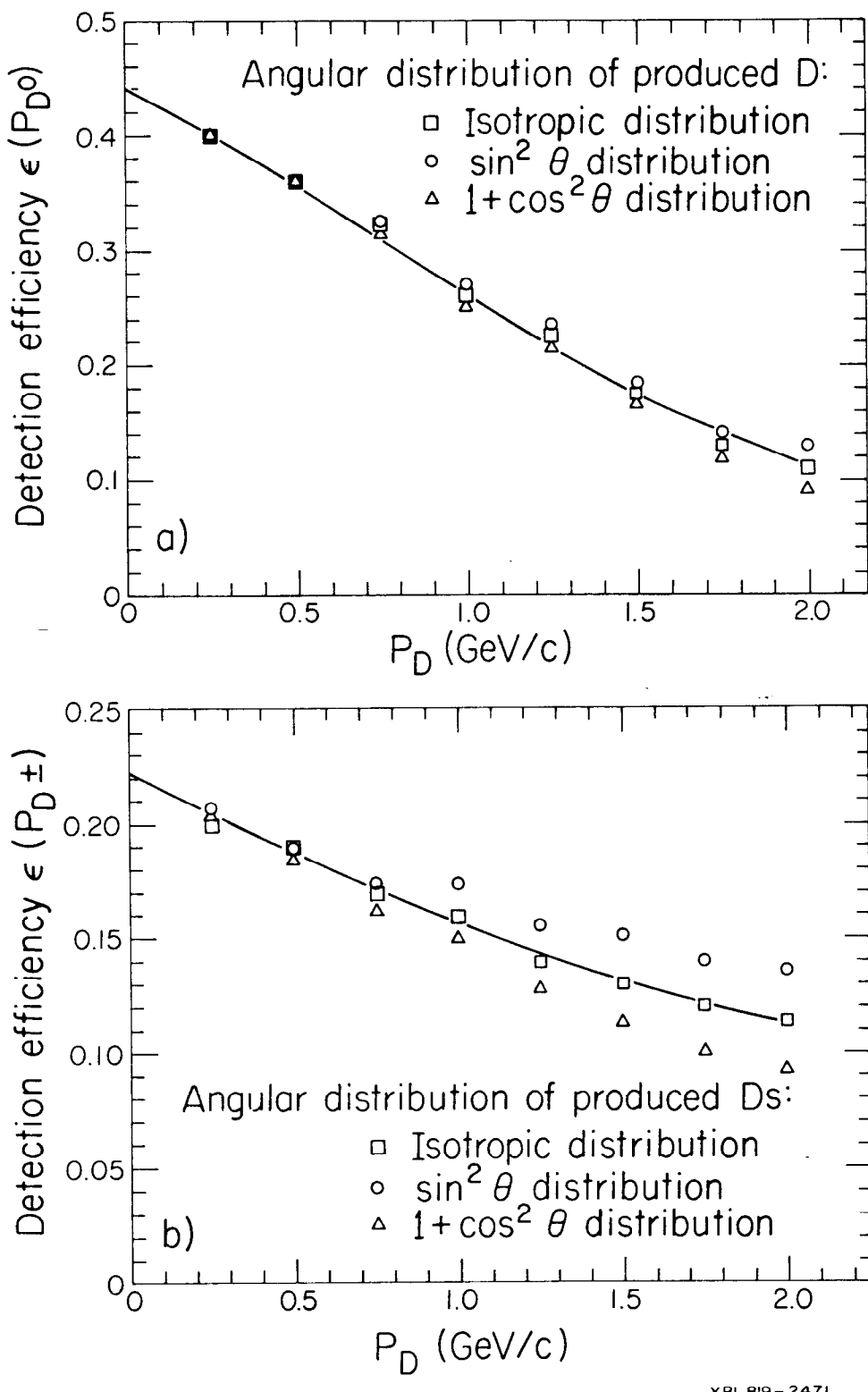
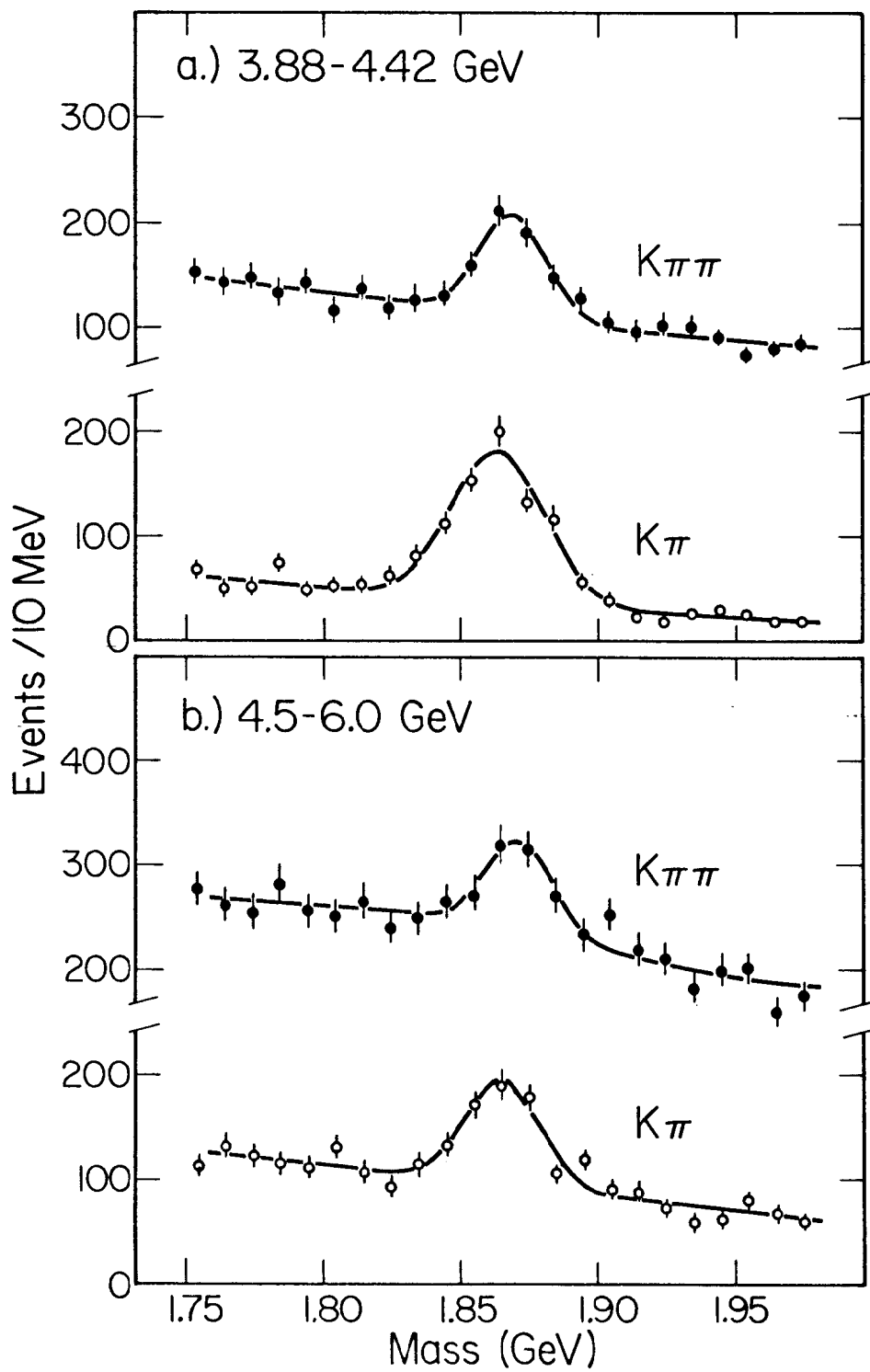
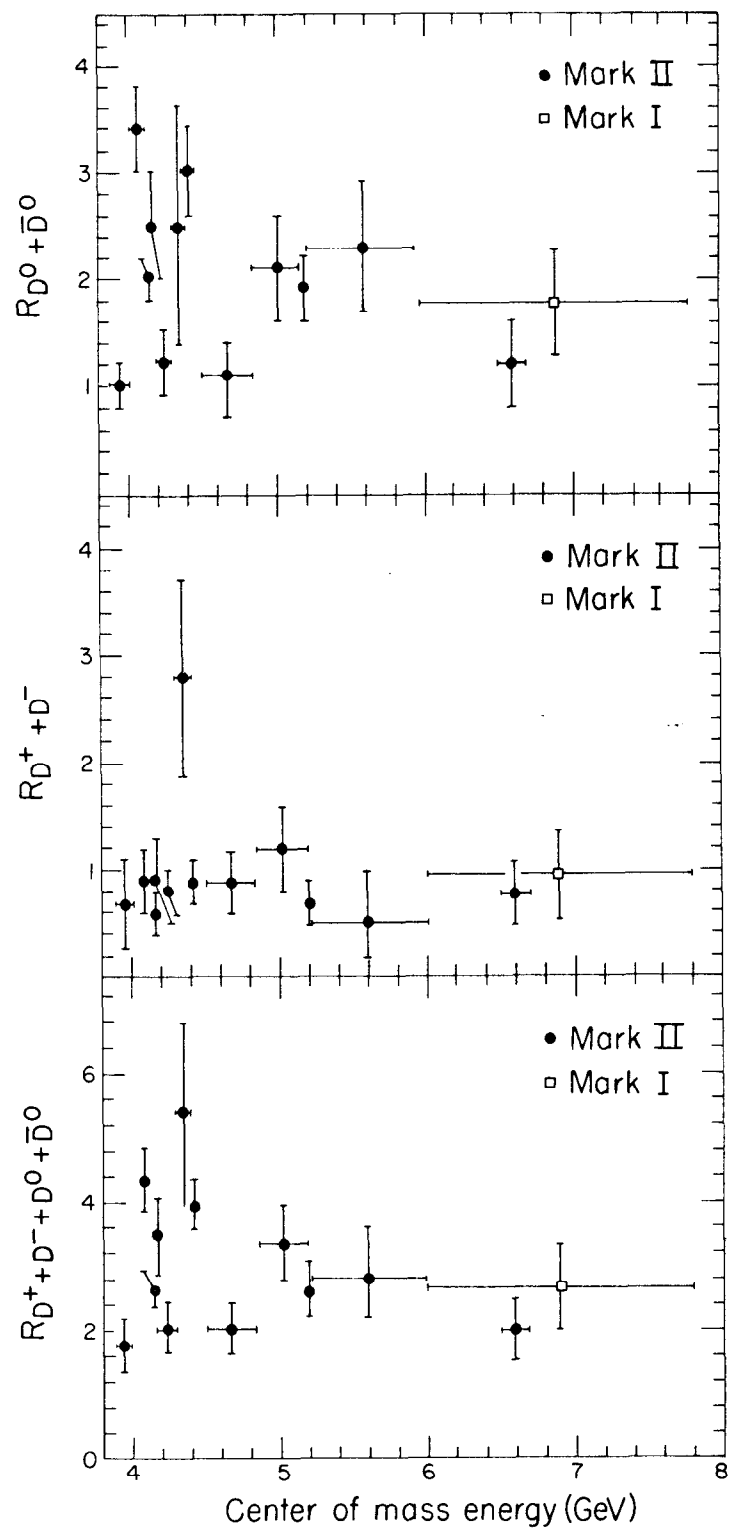


Fig. 2



XBL 825-692

Fig. 3



XBL 819-2468

Fig. 4

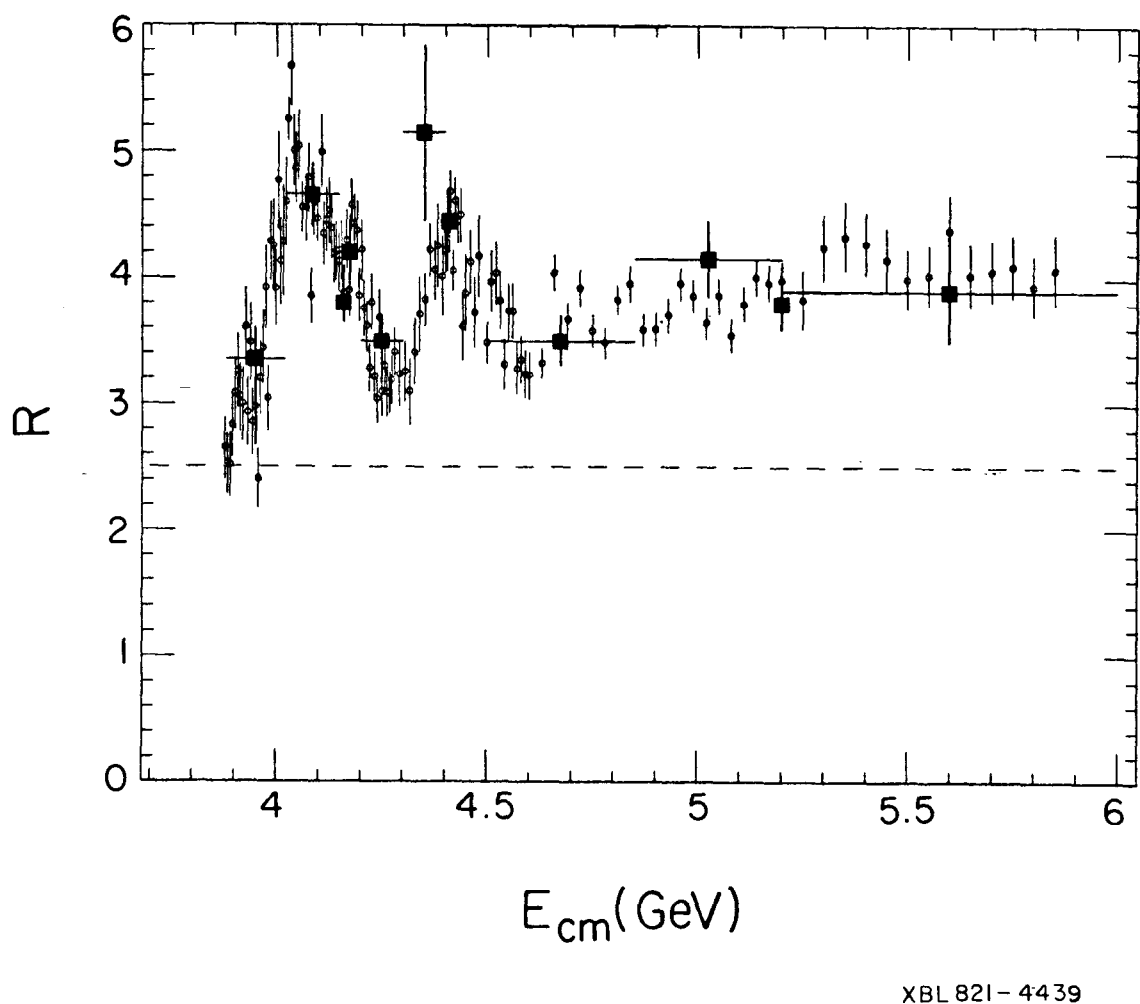
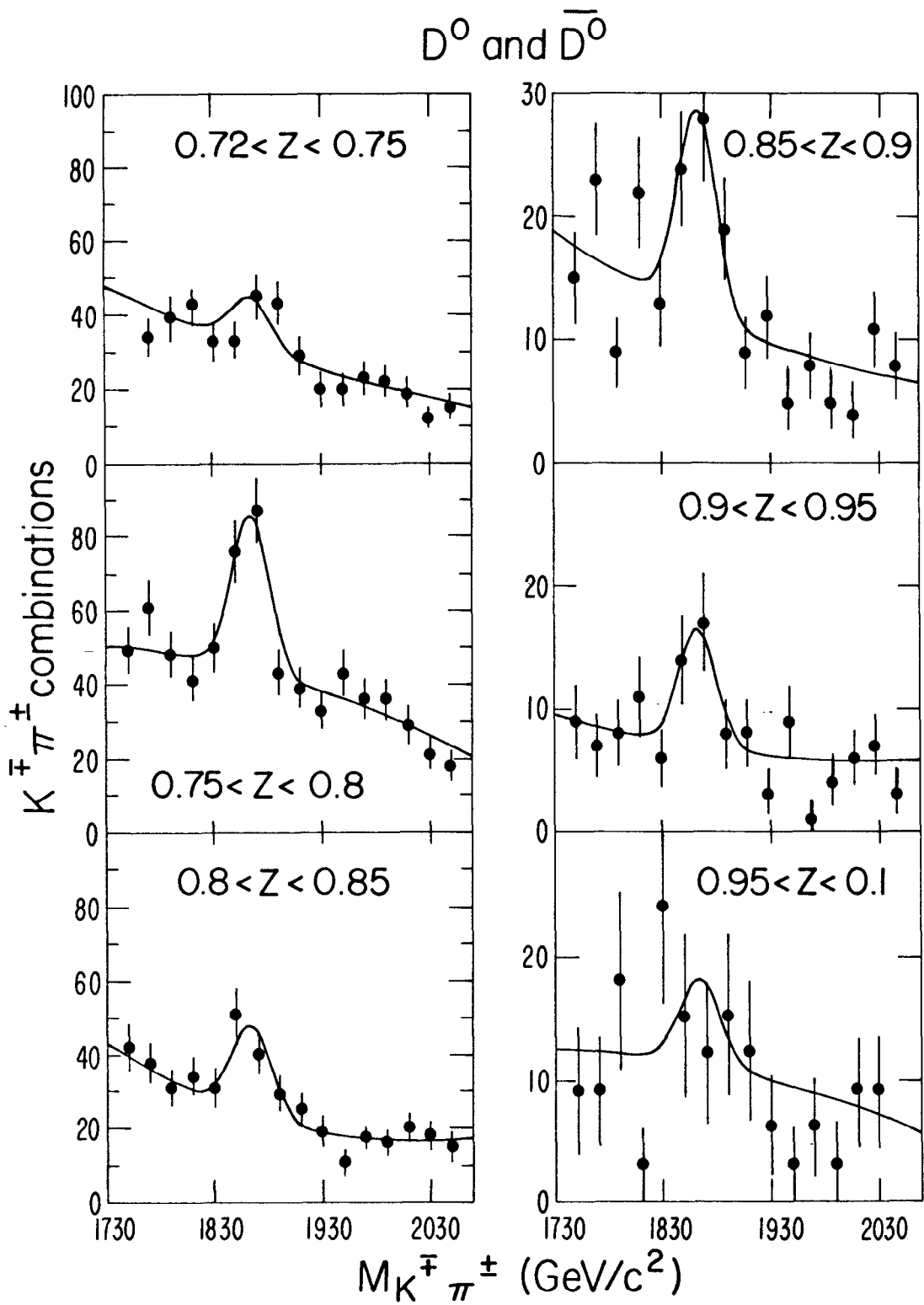
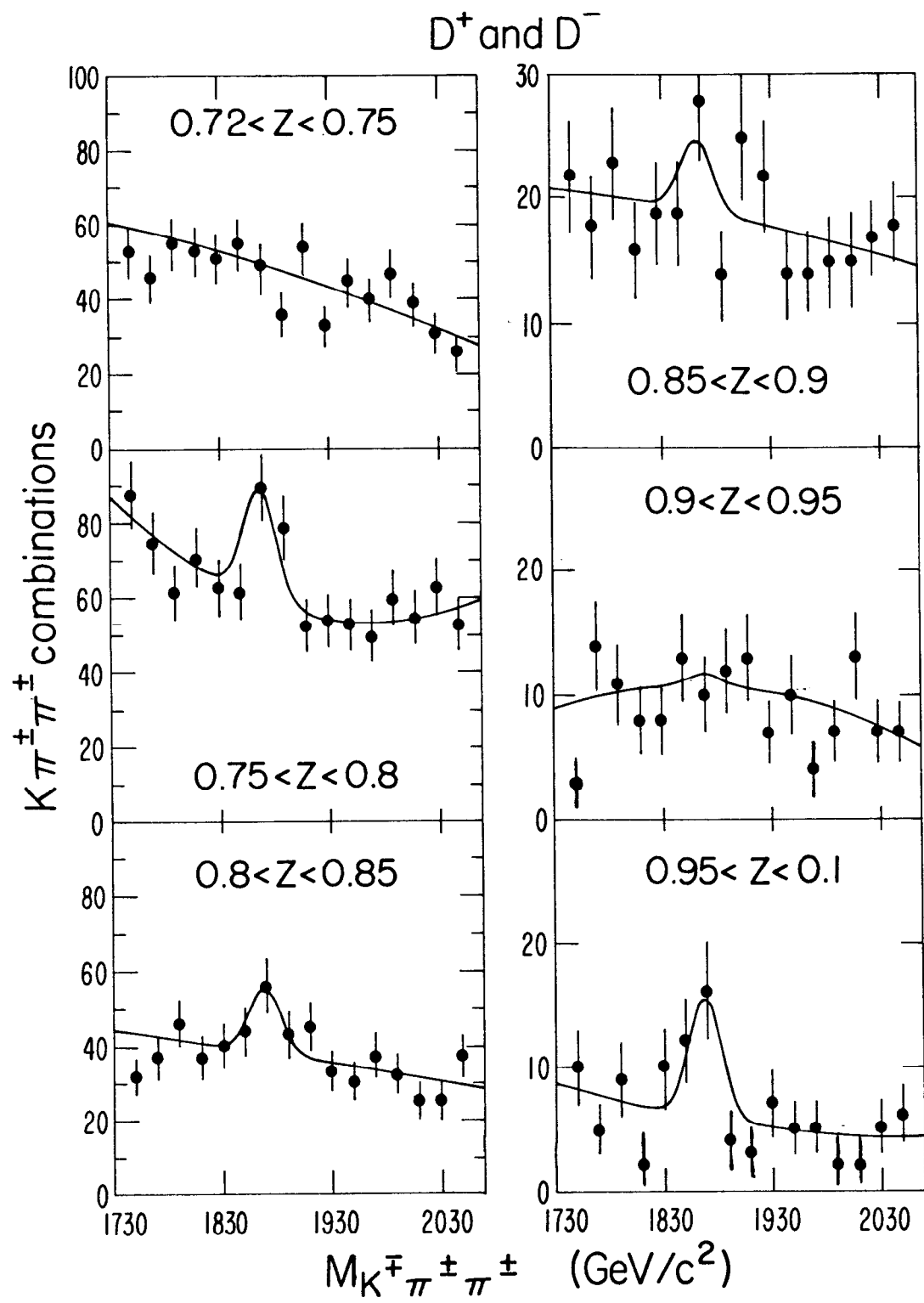


Fig. 5



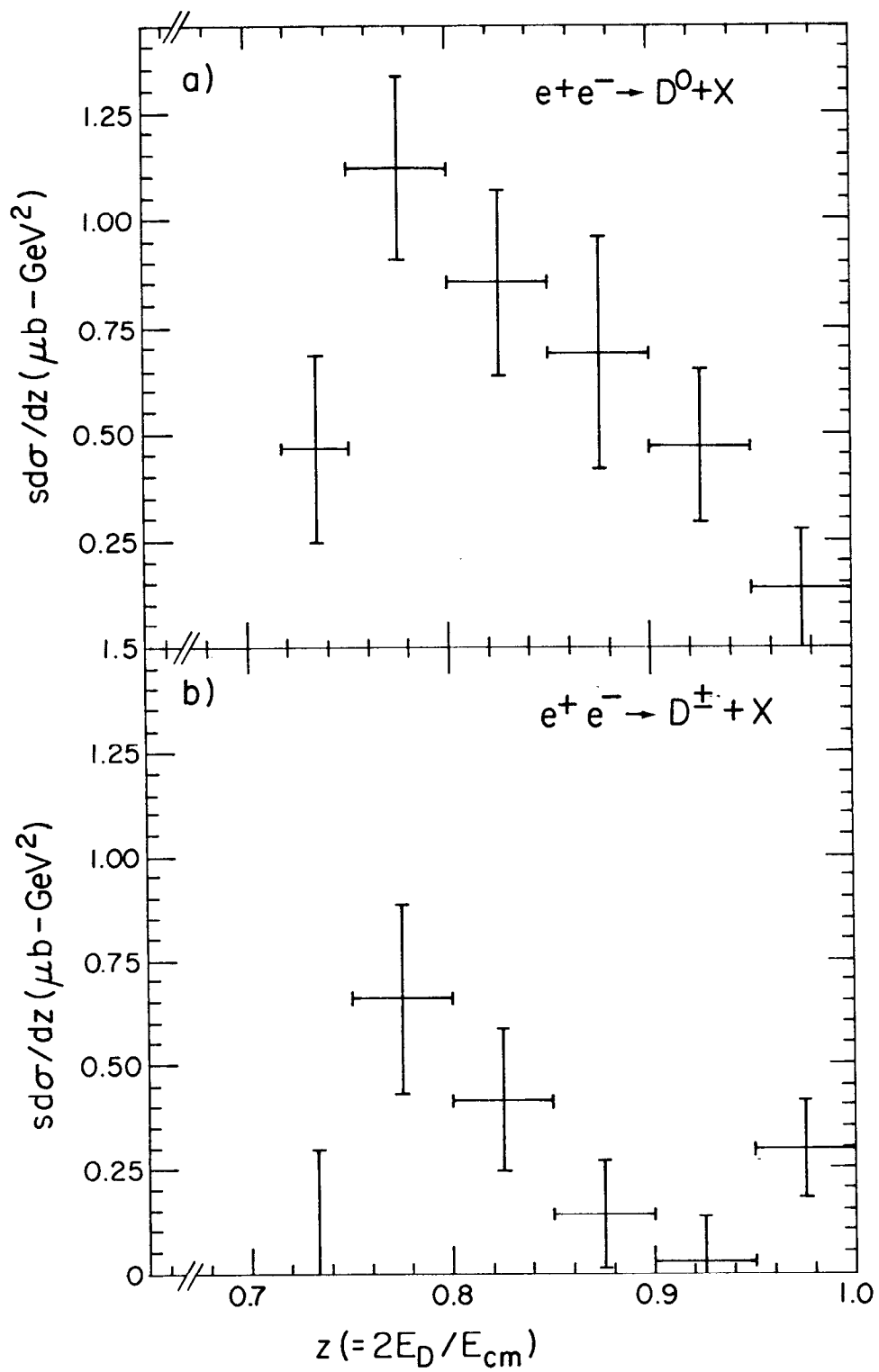
XBL819-2474

Fig. 6



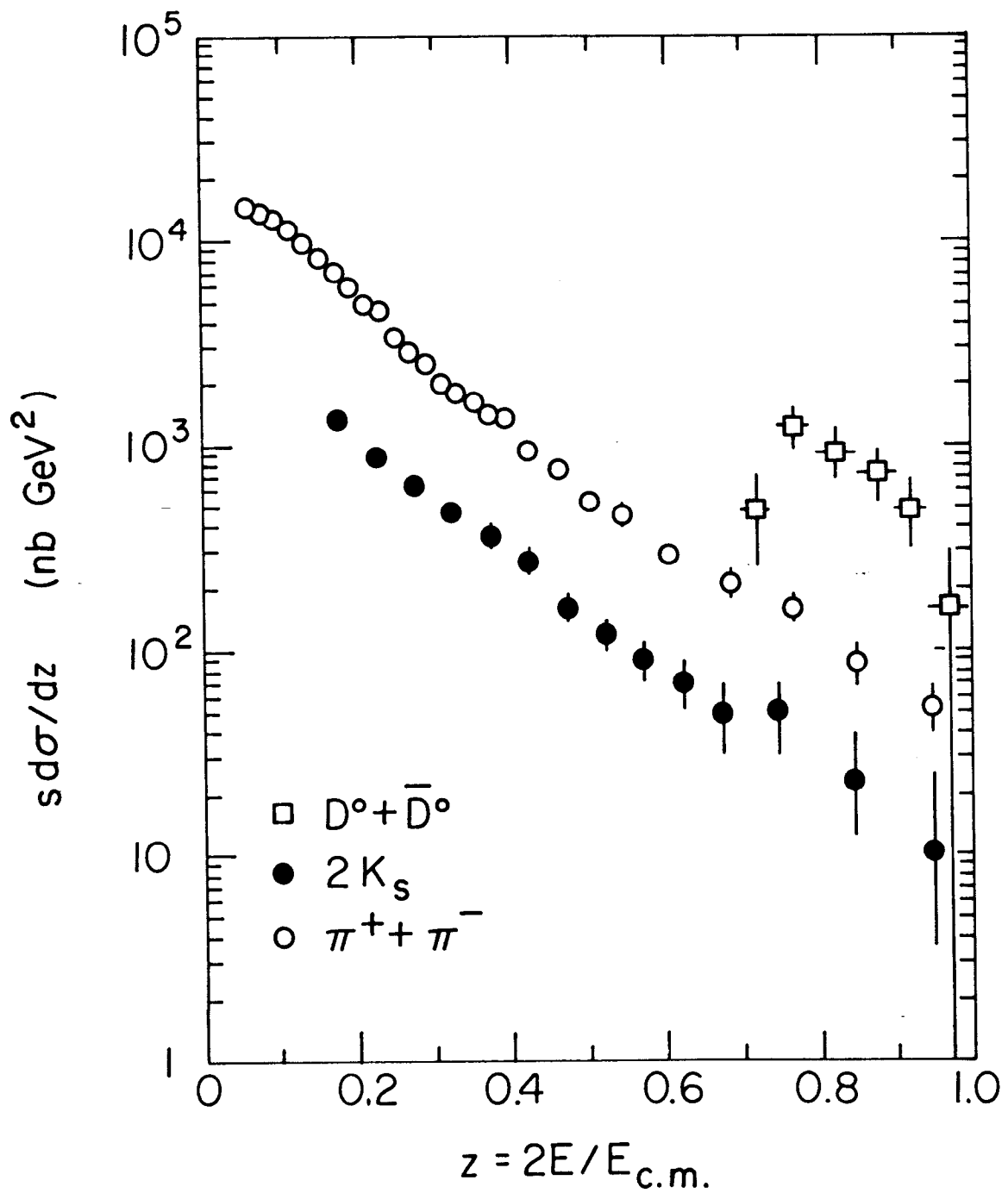
XBL 819-2469

Fig. 7



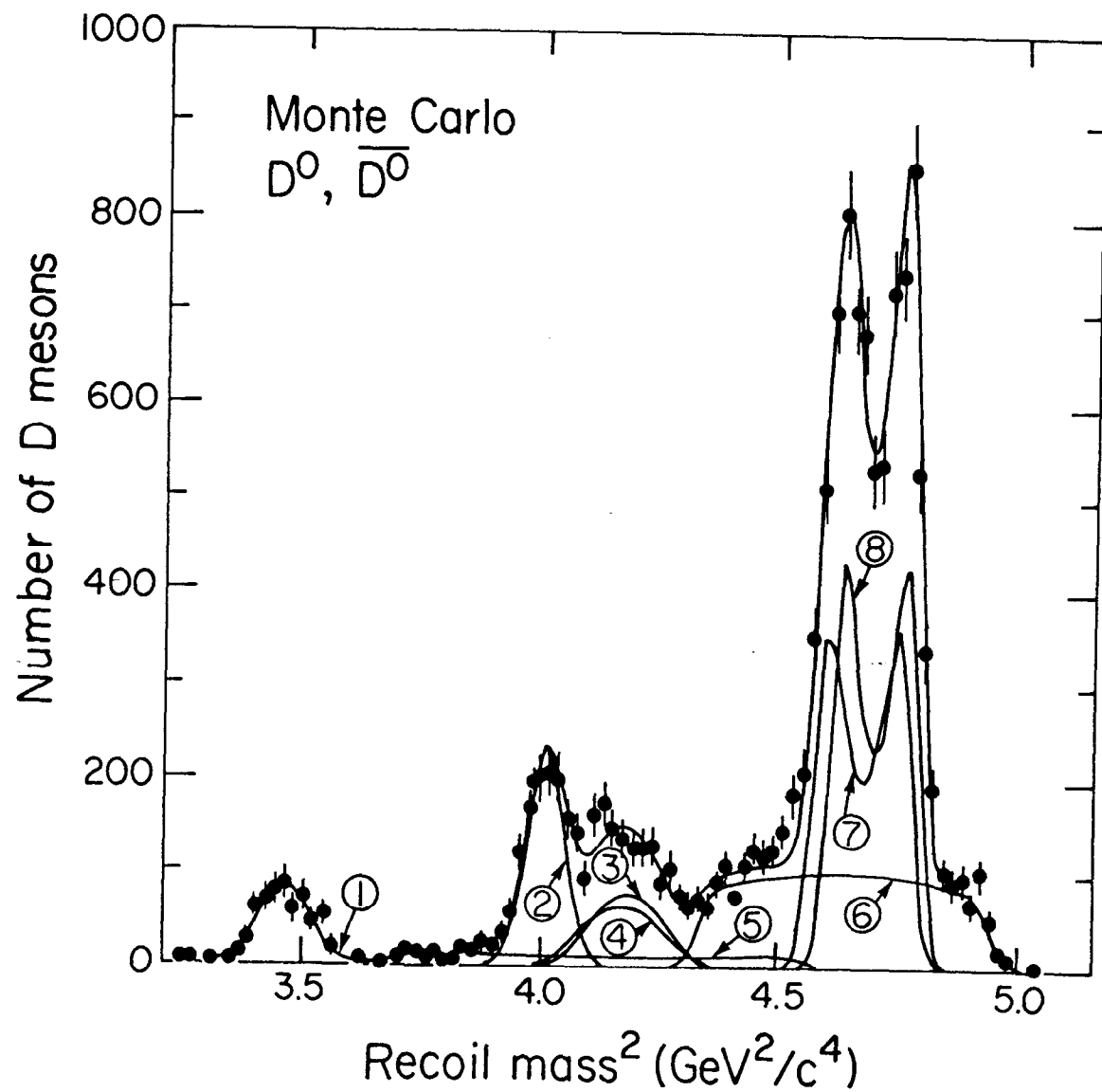
XBL 819-2475

Fig. 8



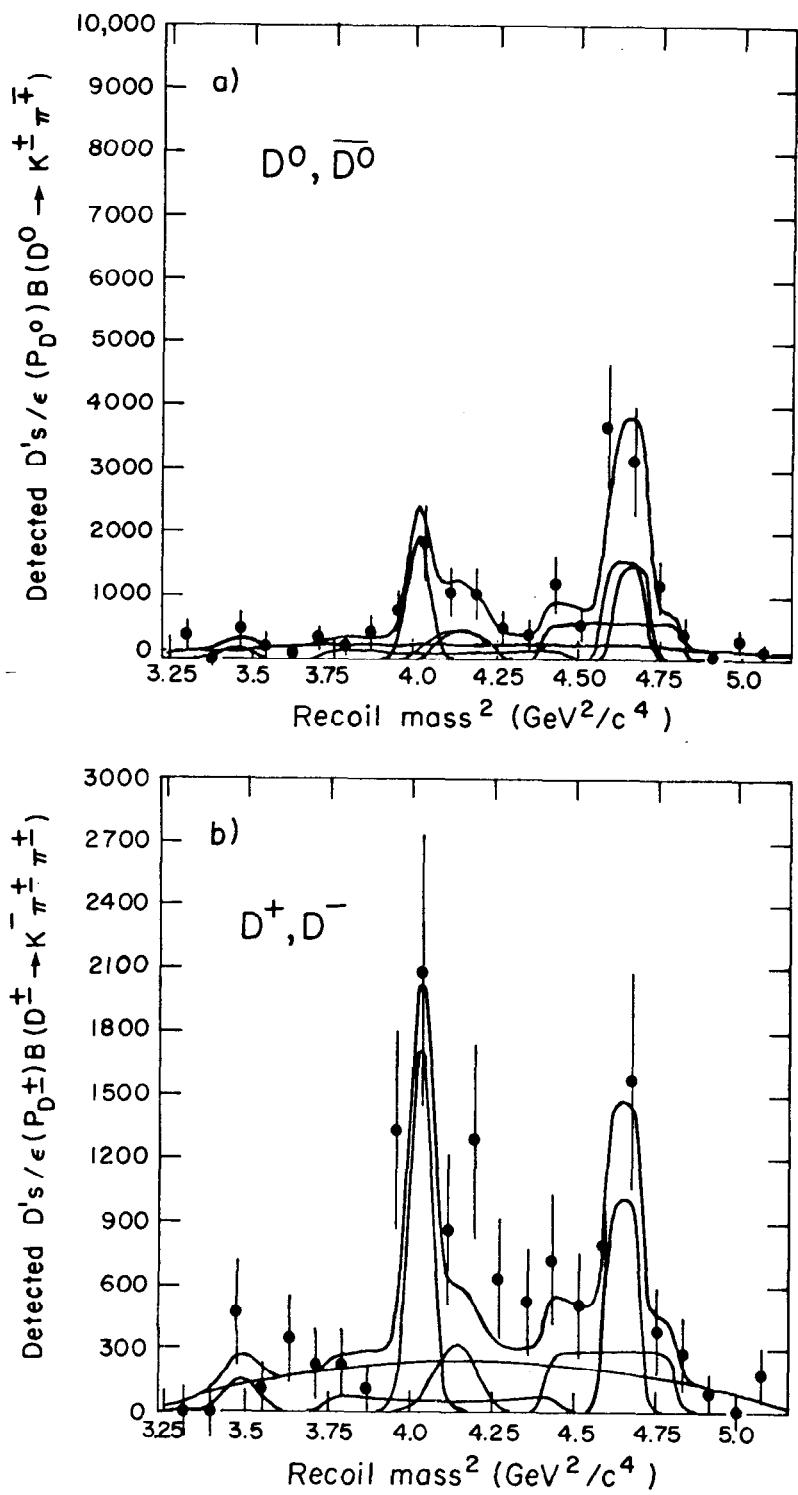
XBL 819-2473

Fig. 9



XBL 819-2472

Fig. 10



XBL 819-2470

Fig. 11

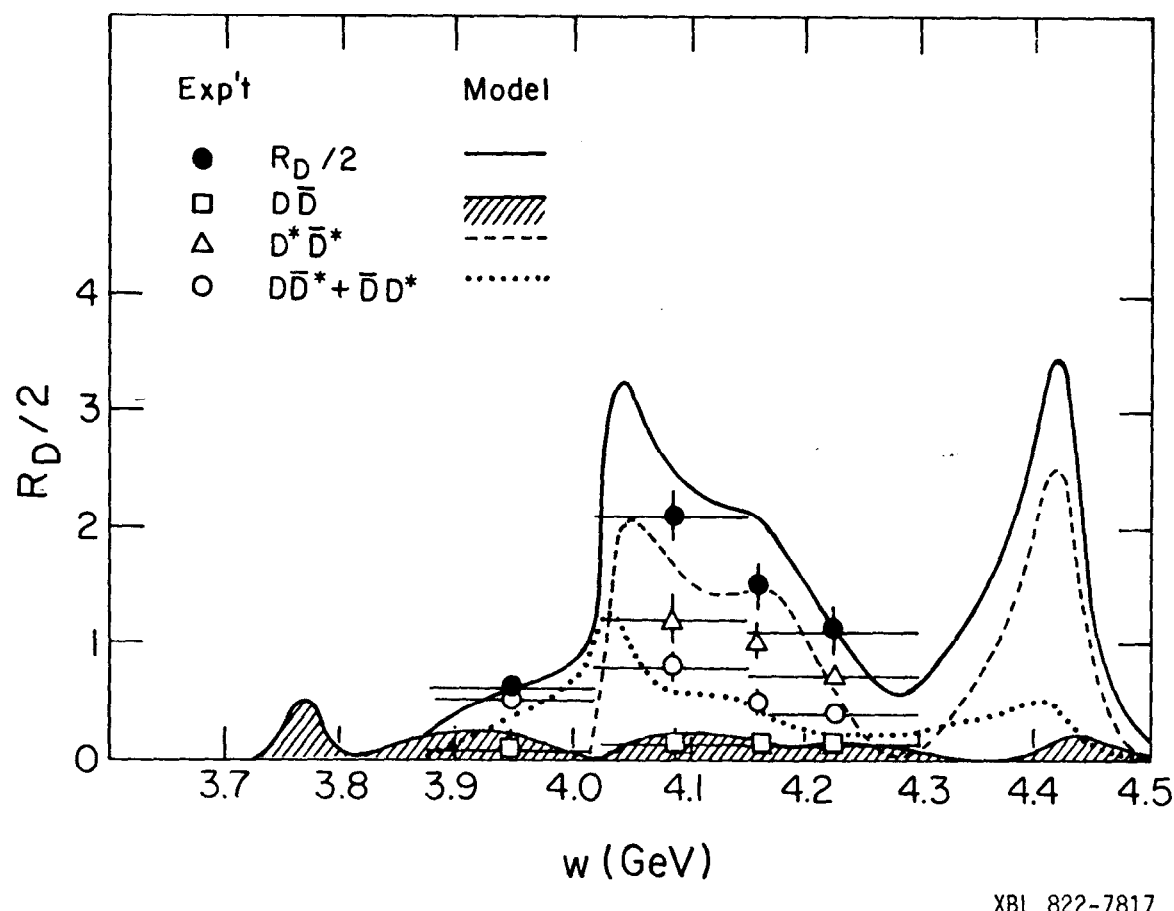


Fig. 12

XBL 822-7817